ARTICLE

Tunable Band Gaps and p-Type Transport Properties of Boron-Doped Graphenes by Controllable Ion Doping Using Reactive Microwave Plasma

Yong-Bing Tang,[†] Li-Chang Yin,[‡] Yang Yang,[†] Xiang-Hui Bo,[†] Yu-Lin Cao,[†] Hong-En Wang,[†] Wen-Jun Zhang,[†] Igor Bello,[†] Shuit-Tong Lee,[†] Hui-Ming Cheng,[‡] and Chun-Sing Lee[†,*]

[†]Center of Super-Diamond and Advanced Films (COSDAF) and Department of Physics and Materials Science, City University of Hong Kong, Hong Kong SAR, People's Republic of China and [‡]Shenyang National Laboratory for Materials Science (SYNL), Institute of Metal Research (IMR), Chinese Academy of Sciences, Shenyang 110016, People's Republic of China

ABSTRACT

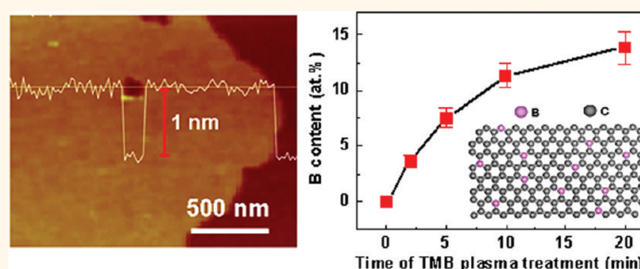

We report tunable band gaps and transport properties of B-doped graphenes that were achieved *via* controllable doping through reaction with the ion atmosphere of trimethylboron decomposed by microwave plasma. Both electron energy loss spectroscopy and X-ray photoemission spectroscopy analyses of the graphene reacted with ion atmosphere showed that B atoms are substitutionally incorporated into graphenes without segregation of B domains. The B content was adjusted over a range of 0—13.85 atom % by controlling the ion reaction time, from which the doping effects on transport properties were quantitatively evaluated. Electrical measurements from graphene field-effect transistors show that the B-doped graphenes have a distinct p-type conductivity with a current on/off ratio higher than 10^2. Especially, the band gap of graphenes is tuned from 0 to ∼0.54 eV with increasing B content, leading to a series of modulated transport properties. We believe the controllable doping for graphenes with predictable transport properties may pave a way for the development of graphene-based devices.

KEYWORDS: graphene · controllable doping · tunable band gaps · p-type transport properties · boron-doped · microwave plasma

Graphene, as individual sheets of carbon atoms bonded in a honeycomb lattice, has unique structure and electronic properties and has been broadly investigated in electronics,[1−5] composites,[6−8] sensors,[9−11] solar cells,[12−14] and electrode materials.[15−19] However, the absence of a band gap and ambipolar transport in the pristine graphene caused very little progress in the applications of graphene in functional devices.[20] Therefore, it is highly desirable to introduce the band gap to graphene and thus tailor its transport properties for practical devices. A variety of methods have been proposed for introducing a band gap in graphene. For instance, a band gap can be formed in graphene by fabricating confined geometries such as nanoribbons,[3,21,22] quantum dots,[23] and nanomesh.[24] A band gap of 200 meV has been observed in bilayer graphene by application of an external electric field.[25] Combining graphene with particular substrates was also found to induce the formation of a band gap in graphene.[26,27] Although these methods can open up a band gap in graphene, they are far away from the practical applications due to their poor controllability and complex process. For example, there is no facile means for the formation of a graphene layer that can be exfoliated from or transferred from the graphene synthesized on SiC,[28] and the width of graphene nanoribbon is required to be narrower than 10 nm to open up its band gap.[22,29,30] Theoretical and experimental studies demonstrated that the intentional doping can modulate the band structure of graphene and open a band gap between the valence and conduction bands, thus tuning the electrical properties.[1−9] Several techniques were reported to incorporate heteroatoms into graphenes through chemical doping, such as electrothermal reactions and chemical vapor deposition.[30−34] However, many doping issues, especially control of doping concentration and corresponding transport properties, remain largely unresolved, so it is difficult to quantify the doping effects yet. Here, we report the

* Address correspondence to apcslee@cityu.edu.hk.

Received for review July 20, 2011 and accepted February 21, 2012.

Published online February 21, 2012
10.1021/nn3005262

© 2012 American Chemical Society

realization of tunable band gaps and transport properties for B-doped graphenes (GS) *via* controllable ion doping using reactive microwave plasma. The doping concentration was adjusted over a wide range by controlling the doping duration. As a result, we can quantify the doping effects in these as-doped GS since both the doping concentration and intrinsic properties are known. The capability of tuning the doping concentration, thus leading to tunable band gaps and electrical properties in GS, is a necessary step for approaching practical devices.

RESULTS AND DISCUSSION

Preparation of B-Doped Graphenes. To quantify the doping effects, it is essential to first understand the pristine transport properties of GS, so we prepared the GS on the SiO_2/Si substrate by the mechanical exfoliation method.[1] The GS samples were first annealed in vacuum to remove surface residues. Then, the GS samples were placed on a stage in a plasma-enhanced CVD chamber (Supporting Information, Figure S1) and reacted with the ion atmosphere of trimethylboron (TMB) decomposed by the low-energy microwave plasma. Five GS samples were prepared with different reaction times of 0, 2, 5, 10, and 20 min with the ion atmosphere of the TMB and denoted as samples BG_0, BG_1, BG_2, BG_3, and BG_4, respectively. It should be noted that the GS sample stage was not directly exposed to the plasma ball to avoid possible etching. The TMB molecule is easy to decompose and form gaseous B atoms and has been widely used for p-doping for diamond and related materials.[35]

Characterizations of B-Doped Graphenes. Atomic force microscopy (AFM) characterizations indicate that the reacted graphenes have a relatively smooth surface after TMB treatment (Figure 1a), similar to that of the undoped GS (Supporting Information, Figure S2). The thickness is in the range of 1.1−1.3 nm, which is similar to the reported AFM results for few-layer graphene sheets, where the height of single-layer graphene is found to be ∼1 nm.[1−5] Combined characterizations of transmission electron microscopy (TEM, Figure 1b), high-resolution TEM (inset, Figure 1b), and electron diffraction pattern (Figure 1c) confirmed that the doped graphenes remained crystalline, similar to a previous report for H-doped graphenes.[36] The boron doping would not result in an obvious structural degeneration of graphenes due to the fact that the length of the B−C bond (1.49 Å) is close to that of the C−C bond (1.43 Å).[37,38] Meanwhile, as reported in previous studies,[39−41] the electronegativity of the B atom is lower than that of the C atom, leading to a lower binding energy of the C−B bonds compared to that of C−C bonds. Especially, the boron doping of graphenes is relatively easy because the formation energy of B-doped graphene from gaseous dopant atoms is about 5.6 eV/atom, which is much lower than that of nitrogen doping (8.0 eV/atom), suggesting that the B doping is more energetically favorable.[37]

Chemical composition and bonding configuration of the treated graphenes were studied by electron energy loss spectroscopy (EELS). Typical EELS spectrum (Figure 1d) of the graphenes reacted with 5 min decomposition atmosphere of TMB shows two distinct features at ∼189.5 and ∼284.7 eV, corresponding to the K-shell ionization edges of B and C, respectively, while the B signal is absent in the untreated graphene, demonstrating that B atoms were incorporated into the graphenes. The distinct $1s\rightarrow\pi^*$ (285 eV) and $1s\rightarrow\sigma^*$ (291 eV) peaks of the C K-edge are characteristic of sp^2-hybridized carbon networks, which is consistent with the previous reports for few-layer graphene or single-walled carbon nanotubes.[42,43] A detailed inspection of the B K-edge (inset, Figure 1d) also shows a discernible π^* peak as well as a σ^* band, suggesting that the B atoms are in the similar sp^2-hybridized state as their C counterparts.[43−45] As reported in previous literature,[42,46−49] the sharply defined π^* peak and broad σ^* structure features of the B K-edge are typical characteristics of sp^2-bonded B atoms in hexagonal BN networks. By comparing the EELS spectrum of B-doped GS with that of h-BN sheets (Figure S5), we found that the B K-edge is consistent with that of h-BN, indicating that the doped B is in the characteristic sp^2-hybridized state as in h-BN, which further proves that most of the B atoms are substitutionally doped in the GS, as schematically illustrated in Figure 1e, although a part of B atoms located at the edge of graphenes cannot be excluded. Additionally, signals associated with other elements such as oxygen (532 eV) were rarely detected in the EELS analyses.

For investigating the doping distributions in more detail, we further performed spatially resolved EELS mappings. The distributions of doped elements with a trace amount were characterized by the EELS mapping in published literature due to the high sensitivity of this technique.[50−52] Figure 2a presents a zero-loss image of a representative B-doped graphene (5 min reaction with decomposition atmosphere of TMB), along with its corresponding C (Figure 2b) and B (Figure 2c) mappings. It can be seen that the C and B elements coexist in the same regions, indicating that B atoms are homogeneously distributed within graphenes without any segregation domains.

The B content of the reacted graphenes was found mainly to depend on the reaction duration with the decomposition atmosphere of TMB. Figure 3a shows X-ray photospectroscopy (XPS) spectra for the samples after 0−20 min of ion reaction with TMB plasma. Besides the C 1s peak at ∼284.5 eV, the B 1s peak at ∼189.7 was observed for the doped samples, while B signal was not detected in the pristine graphenes. The intensity of the B peak was increased by increasing the

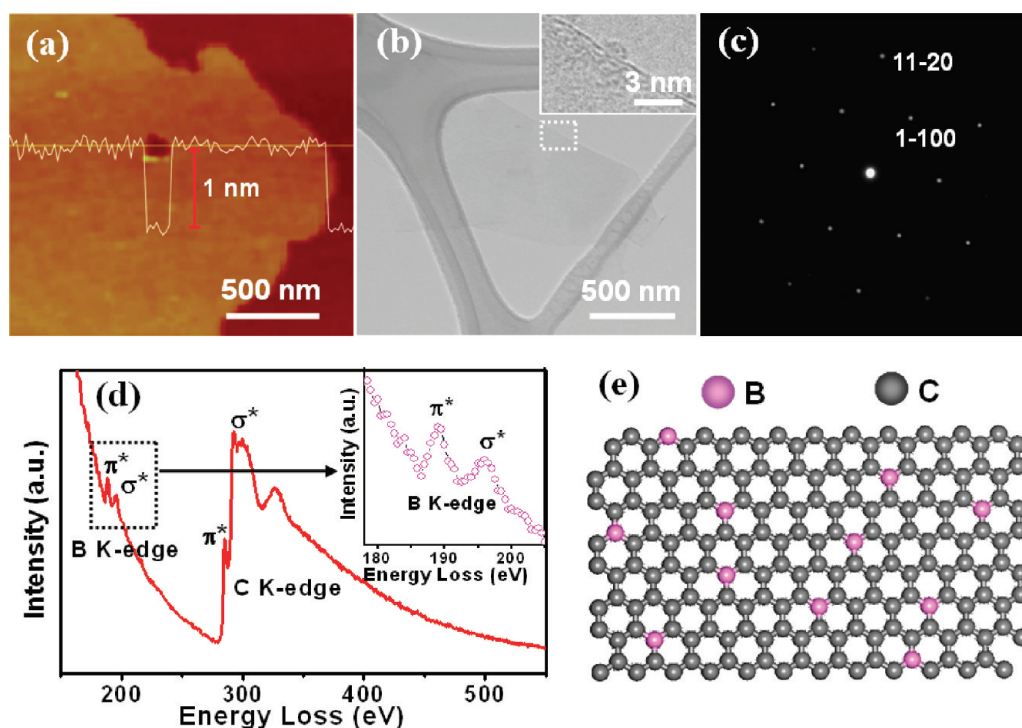

Figure 1. Structure and composition characterizations of the graphenes reacted with 5 min of the B ion atmosphere decomposed from TMB plasma. (a) Typical AFM image of the reacted graphene. (b) TEM image and HRTEM image (inset) of the reacted graphene, and the corresponding SAED pattern (c). (d) Typical EELS spectrum taken from the doped graphenes. (e) Schematic structure of a B-doped graphene with B content of ~6.8 atom %, as detected in the synthesized graphenes.

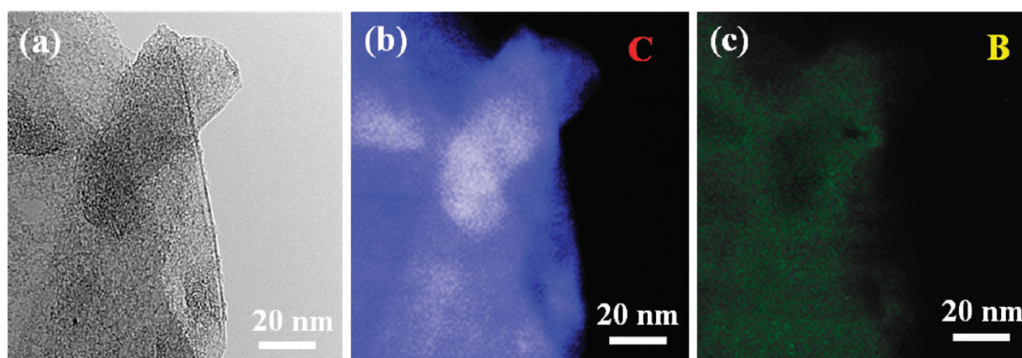

Figure 2. (a) Zero-loss image of an individual graphene from the sample reacted with 5 min of the B ion atmosphere. (b) EELS carbon mapping (blue) of the image shown in (a), and (c) EELS boron mapping (green) of (a). It is clear that the B atoms are distributed uniformly within the doped graphenes.

duration of ion reaction with TMB decomposition gas. Figure 3a,b shows the core-level XPS spectra of C 1s and B 1s for the graphenes with and without ion reaction. It is clear that the C 1s spectra of the doped samples become asymmetric with the increase of the doping duration. On deconvolution, we found two peaks at 283.3 and 284.5 eV, the first corresponding to C–B bond and the second being a feature of the C–C bond (sp^2-hybridization).[53–55] Importantly, the intensity of the C–B bond increased significantly by increasing the reaction time, suggesting that the increase of doping duration leads to higher B content.[53] The B 1s at ~189.7 eV (Figure 3c) for the doped samples can be assigned to the B–C bond, as previously reported,[54,55] which further confirms that the B atoms are substitutionally doped into the graphenes. According to the previous report,[53] the binding energy of the B atoms bonded to the B and C atoms follows the order B–B < B–C due to the electronegativity difference between the two elements B < C. The gradual shift of the B–C bond to higher binding energy as the increase of doping duration also confirms that the boron content in graphenes increases by increasing the reaction time of TMB plasma.

The secondary ion mass spectroscopy (SIMS) measurements were performed to further confirm the B concentration in the doped GS samples. For SIMS measurements, GS suspensions prepared by the mechanical exfoliation

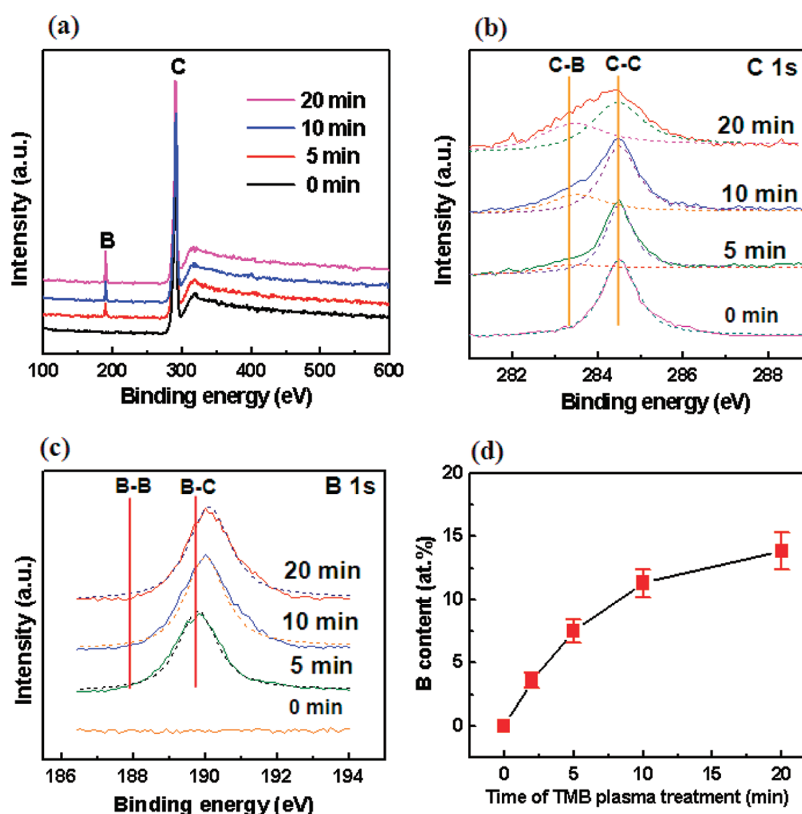

Figure 3. (a) XPS spectra for the samples reacted with different times of the B ion atmosphere. (b) C 1s core-level XPS spectra of the B-doped graphenes. The C 1s bands are fitted by two peaks, C−B at 283.3 eV and C−C at 284.5 eV (dotted lines). (c) B 1s core-level XPS spectra the B-doped graphenes. The B−C bond of doped graphenes gradually shifts to higher binding energy with an increase of the ion reaction time. (d) Dependence of the B content on the ion reaction time measured by the secondary ion mass spectroscopy.

method were dip-coated on Si substrates several times to form a thick GS film (Figure S3). Meanwhile, Si substrates without GS film were also measured to eliminate the influence from the substrate. Prior to SIMS measurements, all samples were annealed at 400 °C in vacuum for 30 min to remove surface residues. The SIMS measurements of the doped GS samples show that the B concentrations are ~3.63, 7.52, 11.31, and 13.85 atom % for doped GS samples BG_1, BG_2, BG_3, and BG_4, respectively, but the B concentration for the undoped GS (BG_0) is lower than 0.01 atom %, demonstrating tha B was indeed incorporated into graphenes by our doping method (Figure S4). On the basis of the SIMS measurements, we found that the boron content increases from 0 to ~13.85 atom % with an increase of the reaction time from 0 to 20 min, as shown in Figure 3d. Although the precise control of the doping concentration is needed to optimize the experimental parameters, this method already showed a strategy for tuning the B doping. Notably, the highest B concentration reported here is significantly higher than the previously reported value (3.1 atom %) for B-doped graphenes *via* the arc-discharge approach using packed boron/graphite electrodes[37] and can be comparable to that of B-doped single-walled carbon nanotubes (20 atom %).[55] The high doping level achieved here is most probably due to the use of gaseous TMB, which can be decomposed easily to form an ion reaction atmosphere, instead of boron powder as the doping precursor.

Although the samples were not directly exposed to the plasma, we believe the forming B ion reaction atmosphere by the microwave plasma is essential for boron doping. As previously reported,[56] the microwave plasma can sufficiently decompose the TMB to form B gaseous ions. When the graphenes were thermally annealed in a decomposition atmosphere of TMB at an appropriate temperature, the surrounding gaseous B ions were expected to adsorb into the graphenes. As demonstrated in the theoretical report,[38] the adsorbed B atoms in GS will undergo a sp^2-hybridization and form C−B bonds with C atoms because the forming energy of the C−B bond is lower than that of the C−C bond for the electronegativity difference between the two atoms B < C.[37] The substitution of B atoms in the hexagonal network will occur within the plane surface through thermal diffusion because the diffusion length of B atoms in graphenes is far larger than the one-atomic thickness.

Electrical Measurements of Undoped and B-Doped Graphenes. To evaluate electrical properties of the B-doped graphenes, we fabricated graphene-based field-effect transistors (FETs) on SiO_2(300 nm)/p^+-Si substrates with Ti/Au (10 nm/20 nm) source−drain

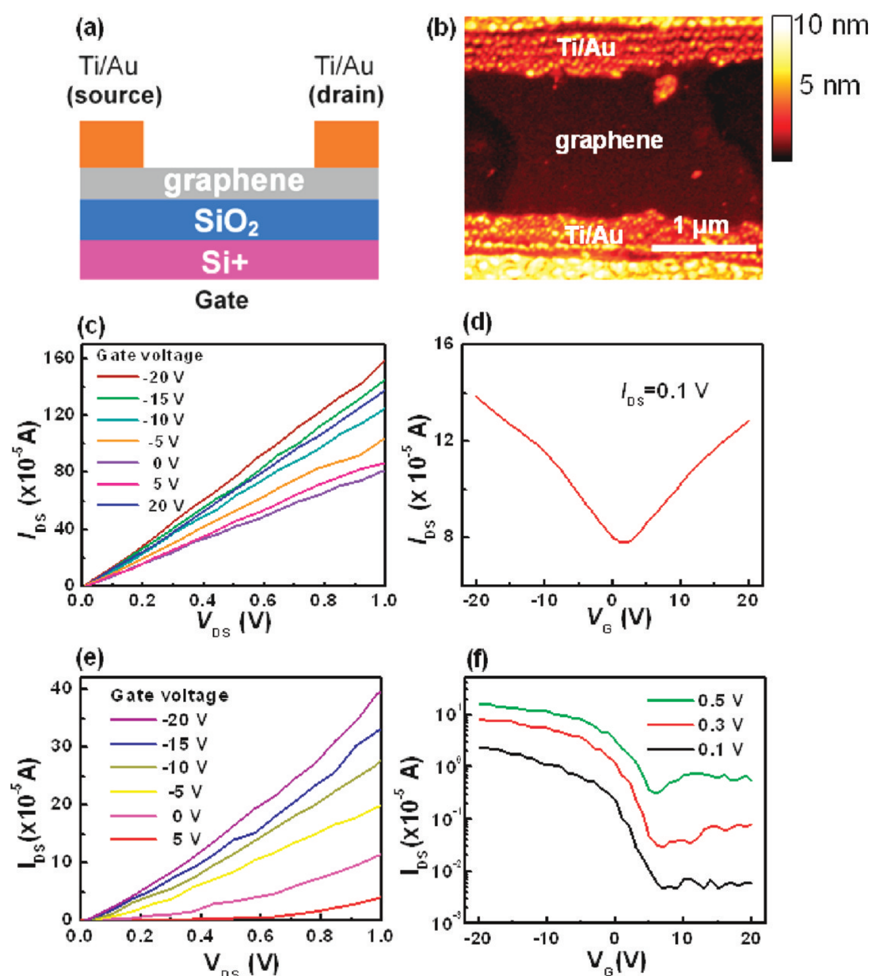

Figure 4. (a) Scheme of bottom-gated graphene FETs. (b) AFM image of a typical FET. (c) $I_{DS}-V_{DS}$ curves of a undoped graphene FET at different V_G. The width of the graphene is ~1.6 μm, and effective channel length is ~1.9 μm. (d) V_G dependence of the I_{DS} measured at V_{DS} = 0.1 V. The I_{DS} shows a bipolar gating effect with a Dirac point near zero V_G. (e) $I_{DS}-V_{DS}$ plots of a typical FET (W ~ 1.2 μm, L ~ 1.7 μm) made of B-doped graphenes reacted with 5 min boron ion atmosphere at different V_G. (f) $I_{DS}-V_G$ curve plot at V_{DS} = 0.1, 0.3, and 0.5 V.

electrodes (Figure S6). The investigation of the electrical properties of graphenes from field-effect transistors is a routine and well-accepted approach.[1−5] The graphene, bridging the source and drain electrodes, behaves as the conducting channel, and gate voltage was applied to the highly doped p-type Si substrate using the standard back-gate geometry. Figure 4 shows a schematic configuration of the FET (Figure 4a) and AFM image of a typical FET with ~2 μm channel length (Figure 4b). The devices were annealed in vacuum before measurement, and all measurements were performed at room temperature.

Figure 4c shows the source−drain current (I_{DS}) *versus* source−drain voltage (V_{DS}) curves obtained from a typical FET (L ~ 1.6 μm, W ~ 1.9 μm, thickness ~ 1.0 nm) made of undoped graphenes at different gate voltages (V_G). The I_{DS} *versus* V_G curve at V_{DS} = 0.1 V (Figure 4d) shows a bipolar gating effect with a Dirac point near zero V_G, as expected for FETs made from pristine graphenes.[1−3] It can be seen that the conductivity remains very high at the neutrality point, which leads to a current on/off ratio <2. The estimated carrier mobilities (μ_e, μ_h) for the undoped graphenes are 3.1−4.5 × 10^3 cm^2/V·s for electrons and 3.3−4.8 × 10^3 cm^2/V·s for holes, respectively.

The transport behavior of graphene was completely changed upon 5 min reaction with the decomposition atmosphere of TMB (~7.5 atom % B). The V_G dependence of $I_{DS}-V_{DS}$ curves (Figure 4e) of the typical FET (L ~ 1.7 μm, W ~ 1.2 μm, thickness ~ 1.2 nm) shows a pronounced characteristic of p-type conductivity; that is, the current of B-doped graphenes decreases with increasing positive V_G. This result suggests that B doping can effectively modulate the transport properties of graphene sheets. The B-doped graphene shows a lower conductivity compared with that of the pristine graphene, presumably because of the lattice defects and strain associated with the boron substitution, similar to previous reports for N-doped graphenes.[31,32] Figure 4f is the I_{DS} *versus* V_G plots for the same device at V_{DS} = 0.1, 0.3, and 0.5 V. The hole mobility μ_h was estimated to be ~550 cm^2/(V·s). Although this value is much lower than that of pristine graphenes, it is higher

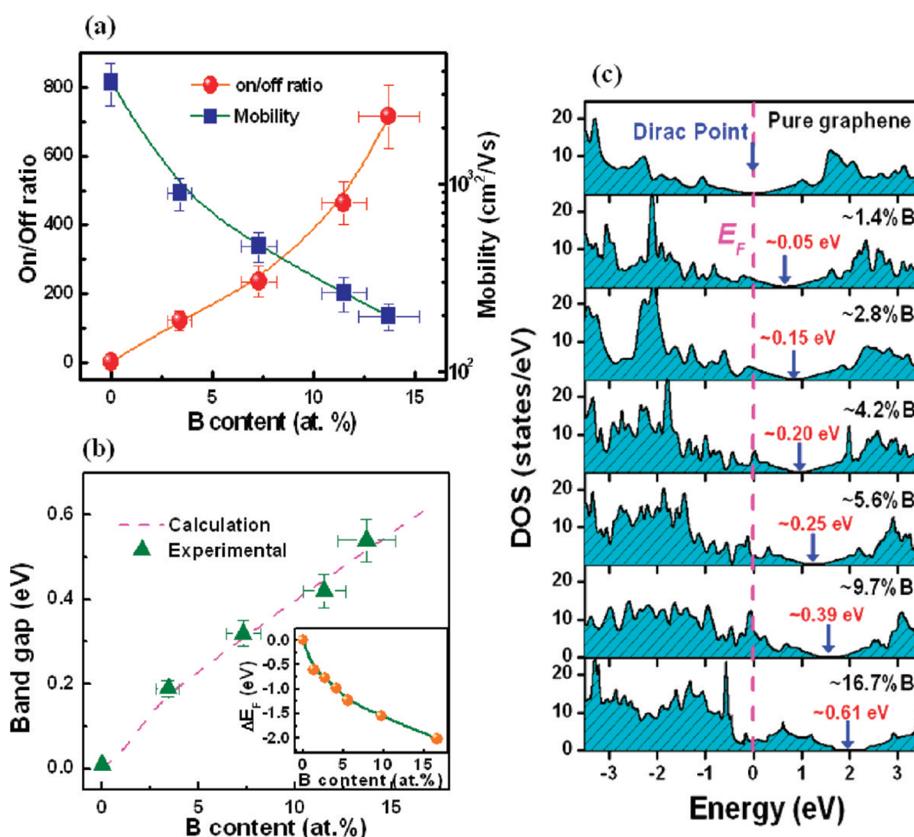

Figure 5. (a) Current on/off and carrier mobility of doped graphenes as a function of the B content. More than 20 FETs were measured for each sample to statistically assess the electrical properties. (b) Experimental band gaps and corresponding calculation results of B-doped graphenes *versus* B content for various FETs. Inset: dependence of doping level (the position of the Fermi level from the Dirac point) on the content of substitutional B. (c) Calculated DOS of graphenes doped with different B content. The Fermi level is labeled by the red dashed line.

than that measured on graphene nanoribbons (100–200 $cm^2/(V \cdot s)$)[6] and reduced graphene oxide (2–200 $cm^2/(V \cdot s)$).[57] According to the previous reports,[29] the band gap of graphenes can be estimated from the plot of on/off ratio *versus* source–drain voltage (delimited by the point of sharply decreasing of on/off ratio value). The current on/off ratio is larger than 200 when V_{DS} is lower than 0.3 V but declines to ~40 when V_{DS} increases to 0.5 V. The V_{DS} dependence of on/off ratio indicates that the on/off ratio of ~210 is maintained before V_{DS} up to 0.32 V (Figure S7), whereas the on/off ratio decreases drastically when the V_{DS} is higher than this value, which suggests that the band gap is about 0.32 V.

Statistical Transport Properties of B-Doped Graphenes. A large number of FETs made from doped graphenes with different B contents were measured to assess the electrical properties with enough statistics. Figure 5a shows the dependence of the on/off ratio and mobility of graphenes on the B concentration. The statistical results showed that the B-doped graphene FETs have a distinct p-type conductivity, and the electrical properties including on/off ratio and mobility were changed by tuning the B concentration. The on/off ratio of undoped GS is in the range of 1–2, whereas the on/off ratio drastically increases to ~120 for BG_1 (~3.6 atom % B), ~230 for BG_2 (~7.5 atom % B), ~460 for BG_3 (~11.3 atom % B), and ~720 for BG_4 (~13.8 atom % B), which clearly shows that the p-type conductivity of B-doped GS can be tuned by adjusting the B concentration. However, the mobility was decreased from ~894 to ~197 $cm^2/(V \cdot s)$ with increasing B content from ~3.6 to ~13.8 atom %. The reduction of electron mobility for B-doped graphenes could be associated with more scattering by the B dopants in the graphenes, as observed in previous reports.[30–34] The band gap *versus* the B content of graphenes is shown in Figure 5b. By using the reported method,[1] we measured band gaps of about 0.19, 0.32, 0.42, and 0.54 eV for the B concentrations of ~3.6, 7.3, 11.3, and 13.8 atom %, respectively, which shows the feasibility of controlling the band gap of graphenes by this doping method.

To get a better understanding of the doping mechanism of B-doped graphenes, we performed first-principles calculations of their electronic densities of states (DOS). In this study, a 7 × 7 graphene supercell, in which one unit containing 71 C atoms, is chosen as a structural model (Figure S8). It means that one B substitutional atom corresponds to a B concentration of ~1.4 atom %. The periodical boundary condition is employed, and the edge of graphene is terminated by H as reported in the literature.[58,59] As measured in the experiments, the B

content was selected in the range of 0−17 atom %. Figure 5c shows the calculated DOS for the undoped and B-doped graphenes. The DOS of undoped graphene shows a semimetal electronic structure with no energy gap at the Fermi level,[1] which is consistent with the experimental observation of the Dirac point near zero. Comparing with the intrinsic graphene, we found that an energy gap of about 0.15 eV appears for the ∼2.8 atom % B-doped graphene. The calculated band gaps are 0, 0.15, 0.20, 0.25, 0.39, and 0.61 eV, respectively, for the selected B concentrations of 0, 1.4, 2.8, 4.2, 5.6, 9.7, and 16.7 atom % (Figure 5c), which demonstrated that the band gap of the B-doped GS is enlarged monotonically with the increase of B concentration, corresponding to the experimental results. Moreover, the p-type doping level (the position of the Fermi level from the Dirac point) was proportional to the concentration of B atoms (Figure 5b, inset). It should be noted that, as with reported calculations,[38,58−63] the band gaps of B-doped GS are different when the B atoms are located at different positions in the structural model, although the B concentration was set at a same value. In addition, the calculated band gap is slightly different for B-doped GS with different configurations (including the shape model and the distance between the doping atoms).[59,61,63] Therefore, the calculations by the first principles provides a the general trend for doping behavior, although the detailed geometry of the B-doped graphenes may slightly change the DOS structure.

CONCLUSIONS

In summary, we demonstrated that the tunable band gaps and transport properties of B-doped graphenes can be achieved through controllable doping by reaction with the ion atmosphere of trimethylboron decomposed by microwave plasma. It was found that the B atoms are substitutionally doped and homogeneously distributed into graphenes without any segregation of B domains. Importantly, the boron content can be well tuned in a wide range of 0−13.85 atom % by adjusting the ion reaction time from 0 to 20 min. The FETs made of B-doped graphenes showed a distinct p-type field-effect behavior with on/off ratios higher than 10^2. Moreover, the band gap of B-doped graphenes was widened from 0 to ∼0.54 eV with the increase of B content, which leads to a series of tunable p-type electrical properties. The doping strategy described here can be extended to controllably dope graphenes with desired elements. We believe that the capability of doping graphenes with predictable transport properties would significantly promote the development of graphene-based devices.

EXPERIMENTAL SECTION

To quantify the doping effects, it is essential to first understand the pristine transport properties of graphenes, so we prepared the monolayer graphenes on the SiO_2/Si substrates by the mechanical exfoliation method.[1] In a typical process, the graphene samples were first annealed at 400 °C in vacuum for 30 min to remove surface residues. Then, the samples were placed on a stage in a CVD chamber and reacted with the ion atmosphere of trimethylboron (TMB) decomposed by the low-energy electron cyclotron resonance (ECR)-enhanced microwave plasma. The sample stage was heated at 300 °C during the doping process. The doping gas was the mixture of TMB and hydrogen (1:9) with a flow rate of 200 sccm. The total pressure was kept at 30 Torr, and the microwave power was maintained at 400 W during the doping process. Five samples were prepared with different reaction times of 0, 2, 5, 10, and 20 min with the decomposition atmosphere of the TMB. Finally, all as-prepared samples were annealed again at 400 °C in vacuum for 30 min before characterizations. It should be noted that the sample stage was not directly exposed to the plasma to avoid possible plasma etching. The TMB molecule is easy to decompose and form gaseous boron atoms and has been widely used for p-doping for diamond and related materials.[35]

The morphology and microstructure of the as-doped graphenes were characterized by atomic force microscopy (AFM), transmission electron microscopy (TEM), high-resolution TEM (HRTEM), and selected area electron diffraction (SAED) pattern. Chemical composition and bonding configuration of the reacted graphenes were studied by electron energy loss spectroscopy (EELS) and X-ray photoemission spectroscopy (XPS).

To evaluate transport properties of the doped graphenes, we fabricated graphene-based field-effect transistors (FETs) on SiO_2(300 nm)/p^+-Si substrates with Ti/Au (10 nm/20 nm) source−drain electrodes by electron-beam evaporation. The graphene, bridging the source and drain electrodes, behave as the conducting channel, and gate voltage was applied to the highly doped p-type Si substrate using the standard back-gate geometry. All FETs were annealed in vacuum at 300 °C for 10 min before electrical measurements. More than 10 devices were tested to confirm statistically the electrical output performance, with all measurements carried out at room temperature.

Conflict of Interest: The authors declare no competing financial interest.

Acknowledgment. The authors thank T. F. Hung, Z. H. Chen, X. Gu, and Y.C. Dong for their kind help in TEM, EELS, SIMS, and *I*−*V* characterizations. The work was supported by the Research Grants Council of Hong Kong (Project No. CityU 101809).

Supporting Information Available: Schematic diagram of the CVD system for ion doping GS, AFM images and statistical thickness for the pristine and B-doped GS, AFM images of GS films for SIMS measurement, SIMS spectra of the B-doped GS, EELS spectrum of the h-BN sheets, photograph of the array of graphene-based FETs and cross-correlation of optical and AFM images of a GS FET, the plot of current on/off ratio *vs* V_{DS} for the FET made of ∼7.5 atom % B-doped GS, and structural model of the GS supercell used for calculations. This material is available free of charge *via* the Internet at http://pubs.acs.org.

REFERENCES AND NOTES

1. Novoselov, K. S.; Geim, A. K.; Morozov, S. V.; Jiang, D.; Zhang, Y.; Dubonos, S. V.; Grigorieva, I. V.; Firsov, A. A. Electric Field Effect in Atomically Thin Carbon Films. *Science* **2004**, *306*, 666–669.
2. Eda, G.; Fanchini, G.; Chhowalla, M. Large-Area Ultrathin Films of Reduced Graphene Oxide as a Transparent and Flexible Electronic Material. *Nat. Nanotechnol.* **2008**, *3*, 270–274.
3. Li, X. L.; Wang, X.; Zhang, L.; Lee, S.; Dai, H. J. Chemically Derived, Ultrasmooth Graphene Nanoribbon Semiconductors. *Science* **2008**, *319*, 1229–1232.

4. Tang, Y. B.; Lee, C. S.; Chen, Z. H.; Yuan, G. D.; Kang, Z. H.; Luo, L. B.; Song, H. S.; Liu, Y.; He, Z. B.; Zhang, W. J.; *et al.* High-Quality Graphenes *via* a Facile Quenching Method for Field-Effect Transistors. *Nano Lett.* **2009**, *9*, 1374–1377.
5. Yang, X. B.; Liu, G. X.; Balandin, A. A.; Mohanram, K. Triple-Mode Single-Transistor Graphene Amplifier and Its Applications. *ACS Nano* **2010**, *4*, 5532–5538.
6. Stankovich, S.; Dikin, D. A.; Dommett, G. H. B.; Kohlhaas, K. M.; Zimney, E. J.; Stach, E. A.; Piner, R. D.; Nguyen, S. T.; Ruoff, R. S. Graphene-Based Composite Materials. *Nature* **2006**, *442*, 282–286.
7. Eda, G.; Chhowalla, M. Graphene-Based Composite Thin Films for Electronics. *Nano Lett.* **2009**, *9*, 814–818.
8. Rafiee, M. A.; Rafiee, J.; Wang, Z.; Song, H. H.; Yu, Z. Z.; Koratkar, N. Enhanced Mechanical Properties of Nanocomposites at Low Graphene Content. *ACS Nano* **2009**, *3*, 3884–3890.
9. Schedin, F.; Geim, A. K.; Morozov, S. V.; Hill, E. W.; Blake, P.; Katsnelson, M. I.; Novoselov, K. S. Detection of Individual Gas Molecules Adsorbed on Graphene. *Nat. Mater.* **2007**, *6*, 652–655.
10. Sudibya, H. G.; He, Q. Y.; Zhang, H.; Chen, P. Electrical Detection of Metal Ions Using Field-Effect Transistors Based on Micropatterned Reduced Graphene Oxide Films. *ACS Nano* **2011**, *5*, 1990–1994.
11. Tang, L. A. L.; Wang, J. Z.; Loh, K. P. Graphene-Based SELDI Probe with Ultrahigh Extraction and Sensitivity for DNA Oligomer. *J. Am. Chem. Soc.* **2010**, *132*, 10976–10977.
12. Liu, Z. F.; Liu, Q.; Huang, Y.; Ma, Y. F.; Yin, S. G.; Zhang, X. Y.; Sun, W.; Chen, Y. S. Organic Photovoltaic Devices Based on a Novel Acceptor Material: Graphene. *Adv. Mater.* **2008**, *20*, 3924–3930.
13. Tang, Y. B.; Lee, C. S.; Xu, J.; Liu, Z. T.; Chen, Z. H.; He, Z. B.; Cao, Y. L.; Yuan, G. D.; Song, H. S.; Chen, L. M.; *et al.* Incorporation of Graphenes in Nanostructured TiO_2 Films *via* Molecular Grafting for Dye-Sensitized Solar Cell Application. *ACS Nano* **2010**, *4*, 3482–3488.
14. Wang, Y.; Chen, X. H.; Zhong, Y. L.; Zhu, F. R.; Loh, K. P. Large Area, Continuous, Few-Layered Graphene as Anodes in Organic Photovoltaic Devices. *Appl. Phys. Lett.* **2009**, *95*, 063302.
15. Wang, X.; Zhi, L.; Mullen, K. Transparent, Conductive Graphene Electrodes for Dye-Sensitized Solar Cells. *Nano Lett.* **2008**, *8*, 323–327.
16. Becerril, H. A.; Mao, J.; Liu, Z.; Stoltenberg, R. M.; Bao, Z. N.; Chen, Y. S. Evaluation of Solution-Processed Reduced Graphene Oxide Films as Transparent Conductors. *ACS Nano* **2008**, *2*, 463–470.
17. Li, X. S.; Zhu, Y. W.; Cai, W. W.; Borysiak, M.; Han, B. Y.; Chen, D.; Piner, R. D.; Colombo, L.; Ruoff, R. S. Transfer of Large-Area Graphene Films for High-Performance Transparent Conductive Electrodes. *Nano Lett.* **2009**, *9*, 4359–4363.
18. Kim, K. S.; Zhao, Y.; Jang, H.; Lee, S. Y.; Kim, J. M.; Kim, K. S.; Ahn, J. H.; Kim, P.; Choi, J. Y.; Hong, B. H. Large-Scale Pattern Growth of Graphene Films for Stretchable Transparent Electrodes. *Nature* **2009**, *457*, 706–710.
19. Bae, S.; Kim, H.; Lee, Y.; Xu, X. F.; Park, J. S.; Zheng, Y.; Balakrishnan, J.; Lei, T.; Kim, H. R.; Song, Y. I.; *et al.* Roll-to-Roll Production of 30-Inch Graphene Films for Transparent Electrodes. *Nat. Nanotechnol.* **2010**, *5*, 574–578.
20. Li, H.; Zhang, Q.; Liu, C.; Xu, S. H.; Gao, P. Q. Ambipolar to Unipolar Conversion in Graphene Field-Effect Transistors. *ACS Nano* **2011**, *5*, 3198–3203.
21. Chen, Z. H.; Lin, Y. M.; Rooks, M. J.; Avouris, P. Graphene Nano-Ribbon Electronics. *Physica E* **2007**, *40*, 228–232.
22. Han, M. Y.; Ozyilmaz, B.; Zhang, Y.; Kim, P. Energy Band-Gap Engineering of Graphene Nanoribbons. *Phys. Rev. Lett.* **2007**, *98*, 206805.
23. Geim, A. K.; Novoselov, K. S. The Rise of Graphene. *Nat. Mater.* **2007**, *6*, 183–191.
24. Bai, J.; Zhong, X.; Jiang, S.; Huang, Y.; Duan, X. Graphene Nanomesh. *Nat. Nanotechnol.* **2010**, *5*, 190–194.
25. Zhang, Y. B.; Tang, T. T.; Girit, C.; Hao, Z.; Martin, M. C.; Zettl, A.; Crommie, M. F.; Shen, Y. R.; Wang, F. Direct Observation of a Widely Tunable Bandgap in Bilayer Graphene. *Nature* **2009**, *459*, 820–823.
26. Rotenberg, E.; Bostwick, A.; Ohta, T.; McChesney, J. L.; Seyller, T.; Horn, K. Origin of the Energy Bandgap in Epitaxial Graphene. *Nat. Mater.* **2008**, *7*, 258–259.
27. Zhou, S. Y.; Gweon, G. H.; Fedorov, A. V.; First, P. N.; de Heer, W. A.; Lee, D. H.; Guinea, F.; Castro Neto, A. H.; Lanzara, A. Substrate-Induced Bandgap Opening in Epitaxial Graphene. *Nat. Mater.* **2007**, *6*, 770–775.
28. Li, X. S.; Cai, W. W.; An, J.; Kim, S.; Nah, J.; Yang, D. X.; Piner, R.; Velamakanni, A.; Jung, I.; Tutuc, E.; *et al.* Large-Area Synthesis of High-Quality and Uniform Graphene Films on Copper Foils. *Science* **2009**, *324*, 1312–1314.
29. Bai, J. W.; Duan, X. F.; Huang, Y. Rational Fabrication of Graphene Nanoribbons Using a Nanowire Etch Mask. *Nano Lett.* **2009**, *9*, 2083–2087.
30. Wang, X. R.; Li, X. L.; Zhang, L.; Yoon, Y. K.; Weber, P. K.; Wang, H. L.; Guo, J.; Dai, H. J. N-Doping of Graphene through Electrothermal Reactions with Ammonia. *Science* **2009**, *324*, 768–771.
31. Guo, B. D.; Liu, Q.; Chen, E. D.; Zhu, H. W.; Fang, L.; Gong, J. R. Controllable N-Doping of Graphene. *Nano Lett.* **2010**, *10*, 4975–4980.
32. Wei, D. C.; Liu, Y. Q.; Wang, Y.; Zhang, H. L.; Huang, L. P.; Yu, G. Synthesis of N-Doped Graphene by Chemical Vapor Deposition and Its Electrical Properties. *Nano Lett.* **2009**, *9*, 1752–1758.
33. Reddy, A. L. M.; Srivastava, A.; Gowda, S. R.; Gullapalli, H.; Dubey, M.; Ajayan, P. M. Synthesis of Nitrogen-Doped Graphene Films for Lithium Battery Application. *ACS Nano* **2010**, *4*, 6337–6342.
34. Qu, L. T.; Liu, Y.; Baek, J. B.; Dai, L. M. Nitrogen-Doped Graphene as Efficient Metal-Free Electrocatalyst for Oxygen Reduction in Fuel Cells. *ACS Nano* **2010**, *4*, 1321–1326.
35. Okushi, H. High Quality Homoepitaxial CVD Diamond for Electronic Devices. *Diamond Relat. Mater.* **2001**, *10*, 281–288.
36. Elias, D. C.; Nair, R. R.; Mohiuddin, T. M. G.; Morozov, S. V.; Blake, P.; Halsall, M. P.; Ferrari, A. C.; Boukhvalov, D. W.; Katsnelson, M. I.; Geim, A. K.; *et al.* Control of Graphene's Properties by Reversible Hydrogenation: Evidence for Graphane. *Science* **2009**, *323*, 610–613.
37. Panchakarla, L. S.; Subrahmanyam, K. S.; Saha, S. K.; Govindaraj, A.; Krishnamurthy, H. R.; Waghmare, U. V.; Rao, C. N. R. Synthesis, Structure, and Properties of Boron- and Nitrogen-Doped Graphene. *Adv. Mater.* **2009**, *21*, 4726–4730.
38. Wu, M.; Cao, C.; Jiang, J. Z. Light Non-metallic Atom (B, N, O and F)-Doped Graphene: A First-Principles Study. *Nanotechnology* **2010**, *21*, 505202.
39. Uddin, M. N.; Shimoyama, I.; Yuji Baba, Y.; Sekiguchi, T.; Nagano, M. X-ray Photoelectron Spectroscopic Observation on B-C-N Hybrids Synthesized by on Beam Deposition of Borazine. *J. Vac. Sci. Technol.* **2005**, *23*, 497–502.
40. Linss, V.; Rodilb, S.; Reinkec, P.; Garnierd, M.; Oelhafend, P.; Kreissige, U.; Richtera, F. Bonding Characteristics of DC Magnetron Sputtered B-C-N Thin Films Investigated by Fourier-Transformed Infrared Spectroscopy and X-ray Photoelectron Spectroscopy. *Thin Solid Films* **2004**, *467*, 76–87.
41. Morant, C.; Prieto, P.; Bareno, J.; Sanz, J. M.; Elizalde, E. Hard BC_xN_y Thin Films Grown by Dual Ion Beam Sputtering. *Thin Solid Films* **2005**, *515*, 207–211.
42. Dato, A.; Radmilovic, V.; Lee, Z.; Phillips, J.; Frenklach, M. Substrate-Free Gas-Phase Synthesis of Graphene Sheets. *Nano Lett.* **2008**, *8*, 2012–2016.
43. Gai, P. L.; Stephan, O.; McGuire, K.; Rao, A. M.; Dresselhaus, M. S.; Dresselhaus, G.; Colliex, C. Structural Systematics in Boron-Doped Single Wall Carbon Nanotubes. *J. Mater. Chem.* **2004**, *14*, 669–675.
44. Borowiak-Palen, E.; Pichler, T.; Graff, A.; Kalenczuk, R. J.; Knupfer, M.; Fink, J. Synthesis and Electronic Properties of B-Doped Single Wall Carbon Nanotubes. *Carbon* **2004**, *42*, 1123–1126.
45. Xu, Z.; Lu, W. G.; Wang, W. L.; Gu, C. Z.; Liu, K. H.; Bai, X. D.; Wang, E. G.; Dai, H. J. Converting Metallic Single-Walled Carbon Nanotnbes into Semiconductors by Boron/Nitrogen Co-Doping. *Adv. Mater.* **2008**, *20*, 3615–3518.

46. Palen, B.; Pichler, T.; Graff, A.; Kalenczuk, R. J.; Knupfer, M.; Fink, J. Synthesis and Electronic Properties of B-Doped Single Wall Carbon Nanotubes. *Carbon* **2004**, *42*, 1123–1126.
47. Kunadian, L.; Andrewsa, R.; Mengu, M. P.; Qian., D. L. Thermoelectric Power Generation Using Doped MWCNTs. *Carbon* **2009**, *47*, 589–601.
48. Golberg, D.; Bando, Y.; Han, W.; Kurashima, K.; Sato, T. Single-Walled B-Doped Carbon, BrN-Doped Carbon and BN Nanotubes Synthesized from Single-Walled Carbon Nanotubes through a Substitution Reaction. *Chem. Phys. Lett.* **1999**, *308*, 337–342.
49. Liao, L.; Liu, K.; Wang, W. L.; Bai, X. D.; Wang, E. G.; Liu, Y. L.; Li, J. H.; Liu, C. Multiwall Boron Carbonitride/Carbon Nanotube Junction and Its Rectification Behavior. *J. Am. Chem. Soc.* **2007**, *129*, 9562–9563.
50. Hayashi, T.; Terrones, M.; Scheu, C.; Kim, Y. A.; Ruhle, M.; Nakajima, T.; Endo, M. Nano Teflons: Structure and EELS Characterization of Fluorinated Carbon Nanotubes and Nanofibers. *Nano Lett.* **2002**, *2*, 491–496.
51. Shuai, M.; Liao, L.; Lu, H. B.; Zhang, L.; Li, J. C.; Fu, D. J. Room-Temperature Ferromagnetism in Cu^{+} Implanted ZnO Nanowires. *J. Phys. D: Appl. Phys.* **2008**, *41*, 135010.
52. Wang, C. Y.; Liu, C. P.; Shen, H. W.; Chen, Y. J.; Kuo, C. L.; Wang, T. Y.; Zheng, R. K.; Ringer, S. P. Growth and Valence Excitations of ZnO:M (Al, In, Sn) Hierarchical Nanostructures. *J. Phys. Chem. C* **2010**, *114*, 18031–18036.
53. Kim, S. Y.; Park, J.; Choi, H. C.; Ahn, J. P.; Hou, J. Q.; Kang, H. S. X-ray Photoelectron Spectroscopy and First Principles Calculation of BCN Nanotubes. *J. Am. Chem. Soc.* **2007**, *129*, 1705–1716.
54. Panchalkarla, L. S.; Govindraj, A.; Rao, C. N. R. Nitrogen- and Boron-Doped Double-Walled Carbon Nanotubes. *ACS Nano* **2007**, *1*, 494–500.
55. Ayala, P.; Plank, W. G.; Grüneis, A.; Kauppinen, E. I.; Rummeli, M. H.; Kuzmany, H.; Pichler, T. A. One Step Approach to B-Doped Single-Walled Carbon Nanotubes. *J. Mater. Chem.* **2008**, *18*, 5676–5681.
56. Zhang, W. J.; Bello, I.; Lifshitz, Y.; Lee, S. T. Recent Advances in Cubic Boron Nitride Deposition. *MRS Bull.* **2003**, *3*, 184–188.
57. Gomez-Navarro, C.; Weitz, R. T.; Bittner, A. M.; Scolari, M.; Mews, A.; Burghard, M.; Kern, K. Electronic Transport Properties of Individual Chemically Reduced Graphene Oxide Sheets. *Nano Lett.* **2007**, *7*, 3499–3503.
58. Cervantes-Sodi, F.; Csanyi, G.; Piscanec, S.; Ferrari, A. C. Edge-Functionalized and Substitutionally Doped Graphene Nanoribbons: Electronic and Spin Properties. *Phys. Rev. B* **2008**, *77*, 165427.
59. Deng, X. H.; Wu, Y. Q.; Dai, J. Y.; Kang, D. D.; Zhang, D. Y. Electronic Structure Tuning and Band Gap Opening of Graphene by Hole/Electron Codoping. *Phys. Lett. A* **2011**, *375*, 3890–3894.
60. Yu, S. S.; Zheng, W. T.; Wang, C.; Jiang, Q. Nitrogen/Boron Doping Position Dependence of the Electronic Properties of a Triangular Graphene. *ACS Nano* **2010**, *4*, 7619–7629.
61. Martins, T. B.; Miwa, R. H.; Silva, A.J. R.; Fazzio, A. Electronic and Transport Properties of Boron-Doped Graphene Nanoribbons. *Phys. Rev. Lett.* **2007**, *98*, 196803.
62. Zhang, Y. H.; Chen, Y. B.; Zhou, K. G.; Liu, C. H.; Zeng, J.; Zhang, H. L.; Peng, Y. Improving Gas Sensing Properties of Graphene by Introducing Dopants and Defects: A First-Principles Study. *Nanotechnology* **2009**, *20*, 185504.
63. Huang, B. Electronic Properties of Boron and Nitrogen Doped Graphene Nanoribbons and Its Application for Graphene Electronics. *Phys. Lett. A* **2011**, *375*, 845–848.